REVIEW

JBMR

Guidelines for Assessment of Bone Microstructure in Rodents Using Micro–Computed Tomography

Mary L Bouxsein,[1] Stephen K Boyd,[2] Blaine A Christiansen,[1] Robert E Guldberg,[3] Karl J Jepsen,[4] and Ralph Müller[5]

[1]Center for Advanced Orthopedic Studies, Beth Israel Deaconess Medical Center and Harvard Medical School, Boston, MA, USA
[2]Department of Mechanical Engineering, Schulich School of Engineering, University of Calgary, Calgary, Alberta, Canada
[3]Parker H Petit Institute for Bioengineering and Bioscience, George W Woodruff School of Mechanical Engineering, Georgia Institute of Technology, Atlanta, GA, USA
[4]Department of Orthopaedics, Mount Sinai School of Medicine, New York, NY, USA
[5]Institute for Biomechanics, ETH Zürich, Zürich, Switzerland

ABSTRACT

Use of high-resolution micro–computed tomography (μCT) imaging to assess trabecular and cortical bone morphology has grown immensely. There are several commercially available μCT systems, each with different approaches to image acquisition, evaluation, and reporting of outcomes. This lack of consistency makes it difficult to interpret reported results and to compare findings across different studies. This article addresses this critical need for standardized terminology and consistent reporting of parameters related to image acquisition and analysis, and key outcome assessments, particularly with respect to ex vivo analysis of rodent specimens. Thus the guidelines herein provide recommendations regarding (1) standardized terminology and units, (2) information to be included in describing the methods for a given experiment, and (3) a minimal set of outcome variables that should be reported. Whereas the specific research objective will determine the experimental design, these guidelines are intended to ensure accurate and consistent reporting of μCT-derived bone morphometry and density measurements. In particular, the methods section for papers that present μCT-based outcomes must include details of the following scan aspects: (1) image acquisition, including the scanning medium, X-ray tube potential, and voxel size, as well as clear descriptions of the size and location of the volume of interest and the method used to delineate trabecular and cortical bone regions, and (2) image processing, including the algorithms used for image filtration and the approach used for image segmentation. Morphometric analyses should be based on 3D algorithms that do not rely on assumptions about the underlying structure whenever possible. When reporting μCT results, the minimal set of variables that should be used to describe trabecular bone morphometry includes bone volume fraction and trabecular number, thickness, and separation. The minimal set of variables that should be used to describe cortical bone morphometry includes total cross-sectional area, cortical bone area, cortical bone area fraction, and cortical thickness. Other variables also may be appropriate depending on the research question and technical quality of the scan. Standard nomenclature, outlined in this article, should be followed for reporting of results. © 2010 American Society for Bone and Mineral Research.

KEY WORDS: MICRO–COMPUTED TOMOGRAPHY; μCT; GUIDELINES; NOMENCLATURE

Purpose of Guidelines

In recent years, the use of high-resolution micro–computed tomography (μCT) imaging to assess trabecular and cortical bone morphology in animal and human specimens has grown immensely. There are now several different commercially available μCT systems, and as a result, there are various approaches to image acquisition, image evaluation, and reporting of outcomes. This lack of consistency makes it difficult to interpret reported results and to compare findings across different studies. Thus the Editor of the *JBMR* (T Clemens) requested that a committee with representatives from Europe, Canada, and the United States be established to address this need for consistent reporting of critical parameters related to image acquisition and analysis and key outcome assessments, particularly for ex vivo analyses of rodent specimens. The committee's draft manuscript was circulated to 15 individuals with expertise in μCT imaging, and their comments were solicited and incorporated into the

Received in original form March 17, 2010; revised form May 11, 2010; accepted May 21, 2010. Published online June 7, 2010.
Address correspondence to: Mary L Bouxsein, PhD, Orthopedic Biomechanics Laboratory RN115, Beth Israel Deaconess Medical Center and Harvard Medical School, 330 Brookline Avenue, Boston, MA 02215, USA. E-mail: mbouxsei@bidmc.harvard.edu

Journal of Bone and Mineral Research, Vol. 25, No. 7, July 2010, pp 1468–1486
DOI: 10.1002/jbmr.141
© 2010 American Society for Bone and Mineral Research

final manuscript. The following guidelines are the product of this committee's work.

These guidelines are not intended to dictate a particular approach for assessing bone microstructure in animal models. The specific experiment and set of research questions will determine the details of the experimental protocol, such as animal age, sex, and genetic background, as well as the skeletal site(s), compartments, and volumes of interest. Rather, these guidelines are designed to provide recommendations regarding (1) standardized terminology and units, (2) what should be included in describing the methods used for a given experiment, and (3) a minimal set of outcome variables that should be reported. Although focused primarily on ex vivo evaluation of isolated bone specimens using desktop μCT systems, the guidelines are intended to be flexible enough to apply to a wide variety of experimental protocols and to accommodate future developments in image acquisition and/or evaluation.

We aimed to establish terminology and guidelines suitable for adoption by the *Journal of Bone and Mineral Research* in its Instructions to Authors in much the same way as those recommended by the Histomorphometry Nomenclature Committee of the American Society for Bone and Mineral Research.[1] Whenever possible, the terminology and units recommended here are consistent with these prior guidelines.[1]

Overview of μCT and Use in Skeletal Phenotyping

Until recently, quantitative histologic techniques were the standard for assessing trabecular and cortical bone architecture. Although histologic analyses provide unique information on cellularity and dynamic indices of bone remodeling, they have limitations with respect to assessment of bone microarchitecture because structural parameters are derived from stereologic analysis of a few 2D sections, usually assuming that the underlying structure is platelike.[1] In comparison, high-resolution 3D imaging techniques, such as μCT, directly measure bone microarchitecture without relying on stereologic models.

First introduced by Feldkamp and colleagues in the late 1980s,[2] μCT now has become the "gold standard" for evaluation of bone morphology and microarchitecture in mice and other small animal models ex vivo. μCT uses X-ray attenuation data acquired at multiple viewing angles to reconstruct a 3D representation of the specimen that characterizes the spatial distribution of material density (Fig. 1). Currently available μCT scanners achieve an isotropic voxel size of as low as a few micrometers, which is sufficient for investigating structures such as mouse trabeculae that have widths of approximately 30 to 50 μm.[3]

The excellent reproducibility and accuracy of μCT measurements of bone morphology have been established in several studies. The accuracy of μCT morphology measurements has been evaluated by comparing them with traditional measures from 2D histomorphometry both in animal[4–8] and in human specimens.[9–13] These studies show that 2D and 3D morphologic measurements by μCT generally are highly correlated with those from 2D histomorphometry. For example, Müller and colleagues

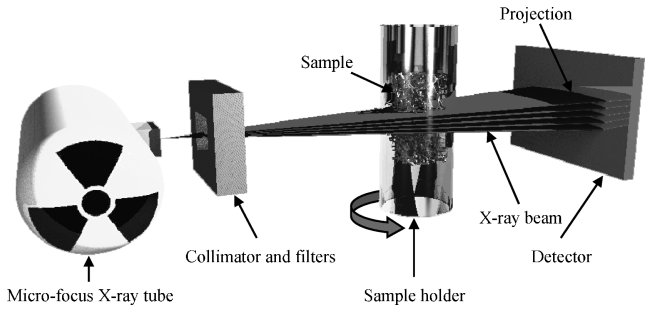

Fig. 1. Key components and operating principle for standard desktop μCT scanner. A microfocus X-ray tube emits X-rays that are collimated and filtered to narrow the energy spectrum. The X-rays pass through the object and are recorded by a 2D charge-coupled device (CCD) array. A full scan involves a set of projections under different rotations of the object. (*Image reproduced with permission from Stauber M, Muller R. Micro-computed tomography: a method for the non-destructive evaluation of the three-dimensional structure of biological specimens. Methods Mol Biol. 2008;455:273-292.*)

reported very high correlations ($r = 0.84$–0.92) and low percent differences between the two methods for measurements of human iliac biopsies.[10] Image resolution, as well as the threshold used to segment the bone from soft tissue, influences these comparisons. Thus some studies report that μCT measures overestimate trabecular thickness relative to histomorphometric measures, an observation that may be attributable to several factors: inadequate resolution of μCT images relative to the trabecular size, the use of a plate model to estimate trabecular thickness in 2D histomorphometry versus direct 3D methods in μCT, poor threshold selection, and/or the fact that 3D μCT measurements of trabecular thickness include trabecular intersections (or nodes), which tend to increase trabecular thickness values compared with measurements made only on trabecular struts.[12] Nonetheless, high correlation between the two techniques provides a strong rationale for the use of μCT to assess skeletal morphometry.

There are numerous advantages to using μCT for assessment of bone mass and morphology in excised specimens: (1) It allows for direct 3D measurement of trabecular morphology, such as trabecular thickness and separation, rather than inferring these values based on 2D stereologic models,[14–16] as is done with standard histologic evaluations, (2) compared with 2D histology, a significantly larger volume of interest is analyzed, (3) measurements can be performed with a much faster throughput than typical histologic analyses of histomorphometric parameters using undecalcified bone specimens, and (4) assessment of bone morphology by μCT scanning is nondestructive; thus samples can be used subsequently for other assays, such as histology or mechanical testing. Finally, μCT scans may be used to provide an estimate of bone tissue mineralization by comparing X-ray attenuation in the bone with that of hydroxyapatite standards, although this must be done with care given the constraints of the polychromatic X-ray source typical for desktop instruments.[17] This voxel-based mineral density data, along with the high-resolution morphology of the bone determined from the μCT scan, also can be used to create micro–finite element (μFE) models to estimate mechanical behavior.[18]

The first study to quantify bone morphology using μCT was an examination of subchondral bone changes in a guinea pig model of osteoarthritis.[19] Since that time, μCT has been used for a wide range of studies of bone mass and bone morphology, including analysis of growth and development,[20] skeletal phenotypes of different mouse strains,[21–23] genetically altered mice,[24–26] and animal models of disease states such as postmenopausal osteoporosis[7,8,23,27] and renal osteodystrophy.[28] Additionally, μCT has been used to assess the effects of pharmacologic interventions,[7,29] as well as mechanical loading[30] and unloading.[31] Furthermore, μCT has been used to image macrocracks in cortical bone,[32] to evaluate fracture healing,[33–38] and in combination with contrast agents to assess 3D vascular architecture[39] and articular cartilage morphology and composition.[40–42] As μCT technology continues to improve and the application of this technique becomes even more ubiquitous, it will become increasingly important to have a standardized set of guidelines pertaining to the reporting of scan parameters and results from μCT studies.

The following sections describe the steps involved in the evaluation of bone morphometry and tissue mineral density by μCT, namely, image acquisition, image processing, image analysis, and reporting of results. In each section, recommendations are made for standardized nomenclature and key variables that should be reported in the methods and results sections of publications. The final section describes the use μCT for purposes other than standard ex vivo bone morphometry measurements.

Image Acquisition

This section describes the key steps and considerations involved in acquiring μCT images, along with recommendations for variables that should be included in the methods section of a paper.

Sample preparation and positioning

The first steps in image acquisition involve preparation and positioning of the sample within the sample holder. Sample preparation will vary with the type of specimen such that neonates may be scanned intact, whereas specimens from older animals will be excised with soft tissues removed. A key concept is to orient the specimens consistently within the sample holder and scanner. Commonly, specimens are aligned with the vertical axis of the scanner, although alignment with the horizontal axis is possible as well. Low-density foam or other nonattenuating material is useful to position the specimen firmly in the sample holder because it is critical that there be no relative movement between the specimen and the sample during the scan.

Scanning medium

It is possible to scan specimens in various media, including saline, ethanol, and neutral buffered formalin, as well as with no medium (ie, in air). Scanning in air affords the highest contrast between the specimen and surrounding medium and may be needed in certain situations. However, the scan medium significantly affects the X-ray attenuation,[43] with measurements in air being significantly different from those in either saline or ethanol. This observation leads to two recommendations: (1) Whenever quantitative measurements of tissue mineral density are done, scan the specimens in a liquid medium such as water, saline, or ETOH, and (2) within an experiment, use the same scanning medium and volume for all specimens that are to be compared.

X-ray energy

An X-ray is a electromagnetic waveform, and the energy of each X-ray photon is inversely proportional to its wavelength. In other words, X-ray photons with longer wavelengths have lower energies than photons of shorter wavelengths.[44] The energy of an X-ray photon, which is produced by accelerated electrons striking the X-ray tube target (eg, tungsten), is expressed as units of electronvolts (eV). Desktop μCT systems produce a polychromatic beam, meaning that the X-ray tube produces a spectrum of photon energies. The highest possible photon energy in that spectrum is equal to the applied electrical potential of the X-ray tube; therefore, the mean photon energy of the beam is always lower. For an X-ray tube operating at 45 keV, the average photon energy of the polychromatic beam is typically about 25 keV. It is acceptable to report the mean photon energy (keV) of the spectrum, but it is usually more convenient to report the applied electrical potential across the X-ray tube (kilovolts or kVp, where p stands for peak voltage).

Typically, μCT systems operate in the range of 20 to 100 kVp,[45] and the attenuation of the X-ray photons as they pass through material can be caused by either absorption or scattering depending on their energy. The interaction of lower-energy X-rays ($<$50 keV) is dominated by the photoelectric effect and depends on the atomic number of the materials. The ability to differentiate bone and marrow is best at low energies; however, because the total attenuation of the X-rays increases, only small objects can be measured at low energies because otherwise noise becomes too large to allow quantitative analysis.[46] The interaction of higher-energy X-rays ($>$90 keV) is dominated by Compton scattering, where the attenuation is approximately proportional to the density of the material. In the medium range of X-ray energy (50 to 90 keV), both the photoelectric effect and Compton scattering contribute to attenuation.[44]

Beam hardening

A fundamental assumption in most μCT systems is that the incident X-ray energy spectrum is equivalent to the X-ray energy spectrum that exits the specimen. However, a consequence of the energy dependence of absorption is that the spectrum of a *polychromatic* X-ray beam, as is used in desktop μCT systems, changes as it passes through a given sample: The lower-energy portion of the beam is preferentially stopped, whereas the high-energy portion passes through more easily. This differential absorption of low- and high-energy photons leads to so-called beam hardening, whereby the average energy of the X-ray beam is increased owing to filtering of lower-energy photons. Beam-hardening effects can be reduced by placing a filter (eg, a thin aluminum foil) or beam-flattening filter in the X-ray path to

narrow the energy spectrum. Mathematical methods can reduce beam hardening further, but these are only approximate because the correction depends on the path length of the beam and material composition of the sample. In general, a rule of thumb for selecting X-ray energy is that a higher energy is needed for thicker and denser samples. Optimizing the absorption contrast can be achieved by experimenting with varying X-ray energies and beam-hardening reduction methods (eg, filters, software). However, it is important to note that the settings must be adjusted to match the object diameter and density,[17,45] implying that optimal settings for a single bone may not be suitable for scanning multiple bones simultaneously or for scanning an object of greater size and/or density. The X-ray energy and approach used for beam-hardening correction must be specified in the methods section.

Intensity

The information content of a voxel depends on the signal-to-noise ratio (SNR), and this is governed by the number of incident photons and the sensitivity of the charge-coupled device (CCD) detector. The tube current is measured in microamperes (μA). The total number of photons for each projection during a tomographic scan depends on the tube current (μA) and the integration time for each projection (ms), as well as the number of times each projection is repeated (frame averaging). The integration time and number of frames per projection directly influence the duration of the scan. Whereas SNR can be improved by increasing the integration time and frame averaging, this comes at the tradeoff of a longer scan time with higher radiation exposure. The radiation dose is proportional to the tube current and duration of X-ray exposure; therefore, frequently the product of these parameters is reported (mAs). Alternatively, tube current (μA), integration time (ms), and frame averaging can be reported independently. Both photon saturation and photon starvation can lead to artifacts in the reconstructed image and should be avoided. Photon starvation is more common and can occur, for example, when a dense material such as an orthopedic screw prevents any photographs from reaching the CCD detector.

Calibration

A calibration phantom is necessary to relate CT values to a mineral-equivalent value, normally in milligrams per cubic centimeter (mg/cm^3) of calcium hydroxyapatite (HA) from a solid-state phantom. Owing to the excellent linearity of modern μCT systems, calibration is possible with only two points, although some manufacturers use up to five points, covering a range from 0 up to 1000 mg/cm^3 HA.[46] Measurements of tissue density or apparent density should be reported in milligrams per cubic centimeter of HA rather than CT values to minimize manufacturer dependency (different systems often use different CT-value scales). Many factors (eg, beam-hardening correction, etc.) can influence density results, and absolute differences between scanners cannot be eliminated; however, with care, good relative measures can be made within any given study. Another aspect of calibration usually performed by the manufacturer is the measure of a thin wire (usually tungsten) for determining in-plane spatial resolution via the modulation transfer function (MTF), as well as a method to ensure that geometric inputs to the reconstruction algorithm are correct. Calibration should be performed routinely according to the manufacturer's recommendations.

Voxel size and image resolution

A *voxel* is the discrete unit of the scan volume that is the result of the tomographic reconstruction. It is a 3D volume representing two dimensions within the slice and the slice thickness. Typically, voxels from μCT images have all three dimensions equal and therefore are described as *isotropic* voxels. Ideally, the smallest voxel size (ie, highest scan resolution) available would be used for all scans; however, higher-resolution scans require longer acquisition times because they must collect more projections and generate large data sets. Therefore, the tradeoff between voxel size and scan time should be carefully considered. Differences in voxel size (eg, 10 to 20 μm) have little effect on the evaluation of structures with relatively high thickness (ie, 100 to 200 μm), such as cortical bone or trabeculae in humans or large animal models. However, when analyzing smaller structures such as mouse or rat trabeculae with approximate dimensions of 20 to 60 μm, voxel size can have significant effects on the results.[47] Scanning with low resolution (large voxel size, $>$100 μm) relative to the size of the structure of interest can cause an underestimation of bone mineral density owing to partial-volume effects and overestimation of object thickness (Fig. 2). Generally, as the ratio of voxel size to object size decreases, so does the measurement error regardless of scale (ie,

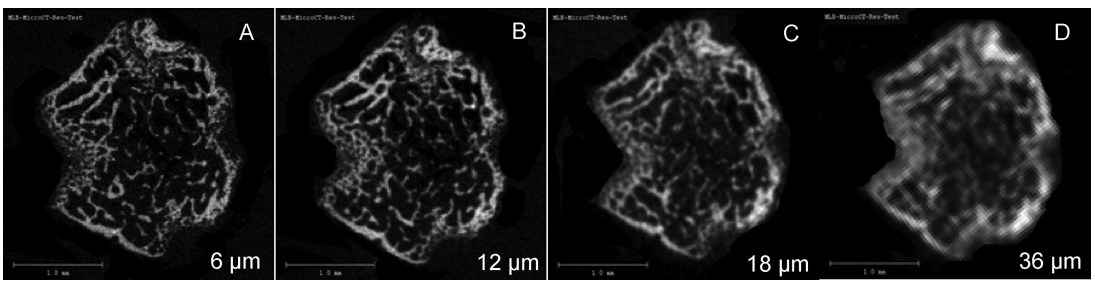

Fig. 2. Effect of voxel size on image quality. 2D gray-scale images of the distal femur of an adult mouse scanned at voxel size of (*A*) 6 μm, (*B*) 12 μm, (*C*) 18 μm, and (*D*) 36 μm. Images acquired at 70 kVp, 114 mA, and 200-ms integration time. (*Images courtesy of Rajaram Manoharan, Beth Israel Deaconess Medical Center.*)

from mouse to human). The minimum ratio of voxels to object size is 2, but this is associated with substantial local errors (albeit smaller when averaged over an entire structure). Ideally, the ratio should be higher for accurate morphologic measurements. The local solution accuracy of μCT based finite-element models is also influenced by voxel size, and a minimum discretization of three to four elements across the thickness of individual trabeculae is recommended to minimize numerical errors.[48]

Finally, it should be made clear that voxel size is not equivalent to spatial resolution of the μCT image. In radiologic physics, CT spatial resolution typically is reported from measurement of the modulation transfer function (MTF).[49] Nevertheless, no standardized approach has been accepted by μCT device manufacturers in reporting spatial resolution. The relationship between spatial resolution and voxel size depends on several factors (ie, mean absorption of sample, detector noise, reconstruction algorithm, X-ray focal spot size and shape, detector aperture, and scanner geometry), and thus it is more appropriate to report voxel size directly. Therefore, one should report the *nominal isotropic resolution* or *isotropic voxel size* to reflect that it is not true spatial resolution.

Region of interest

When setting up the scan acquisition, it is critical to ensure that a sufficient amount of the sample is scanned to allow for reliable and reproducible morphology and density measurements. The region of interest (ROI) should be defined based on the location of the start point of the scan or the contoured region of interest and the size (ie, length) of the region. The starting point should be defined as an absolute (millimeters) or relative distance (percent) from a reproducible landmark, such as the proximal tibial plateau, the metaphyseal growth plate, the mid-diaphysis, or another suitable anatomic site. The size of the scan region should be defined as the distance (eg, proximal or distal) from that start point. Distances should be reported in SI units (millimeters or micro meters); the number of slices can be determined easily knowing the voxel size.

Assessing trabecular bone requires a suitable ROI, and particular consideration should be paid to the distance that the ROI extends into the diaphysis of long bones (which is primarily cortical bone). Extension of the ROI too far into the diaphysis will decrease the mean bone volume fraction relative to an ROI that is contained in the metaphyseal region. To represent trabecular bone architecture accurately, the ROI should contain at least three to five intertrabecular lengths.[50] At the mid-diaphysis, 3D cortical thickness measurements must be based on an ROI that is longer than the cortex is thick; otherwise, the thickness will be underestimated. (Measurements of cortical thickness using the plate model are not subject to this same restriction.) It is important that the whole sample fit within the scanned region, and it may be useful to provide a figure of a representative bone to illustrate the defined ROI and demonstrate that it represents the selected skeletal site well.

Another important issue pertains to the definition of the ROI when comparing bone specimens of varying size (ie, bone length). The usual goal is to choose an ROI that is anatomically and biomechanically comparable among specimens. Thus, in situations where the bone length differs between groups, a uniformly sized ROI will relatively oversample the shorter bones and undersample the longer bones.[51] In this instance, it may be more appropriate to define the ROI as a percentage of bone length or in reference to easily identified landmarks rather than a constant size.

In summary, the first step in generating reliable bone morphometry data using μCT is the image acquisition itself. At a minimum, the methods section of a paper should delineate the scan medium, X-ray tube potential, and voxel size, as well as provide descriptions of the size and location of the ROI (Table 1).

Image Processing

This section describes key concepts related to post-acquisition processing of image data, including filtration and segmentation.

Filtration

Reconstructed μCT data inherently include signal noise that should be reduced by filtering while maintaining sharp contrast between bone and marrow.[52] Removal of image noise is best

Table 1. Key Parameters for μCT Scan Acquisition

Variable	Description	Standard unit
Voxel size[a]	Three dimensions defining the basic discrete unit of the μCT image	μm^3
X-ray energy	Energy is proportional to the frequency (or 1/λ) of X-ray photons	keV
X-ray tube potential (peak)	Applied peak electric potential of X-ray tube that accelerates electrons for generating X-ray photons	kVp
X-ray intensity	X-ray tube current (μA) or product of current and time (mA · s)	mA · s, μA
Integration time	Duration of each tomographic projection	ms
Frame averaging	Number of repeated measurements at each tomography projection	*n*
Projections	Number of tomographic viewpoints used for reconstruction.	*n*

Note: Variables in boldface should be included in the methods section of a paper. Other variables are optional to include in the text.
[a]For isotropic voxel sizes. If not isotropic, must report in-plane voxel size along with slice thickness.

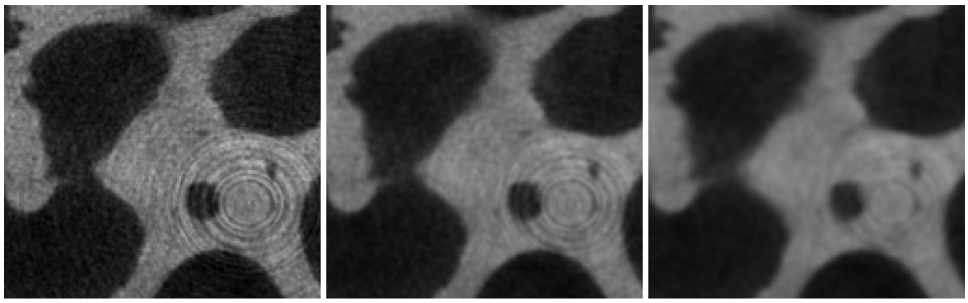

Fig. 3. Effect of Gaussian filtration on image clarity and contrast. As the Gaussian filter width is increased, noise is reduced, and the ring artifacts also can be removed. However, the images are also blurred, and contrast is reduced. (*Image reproduced with permission from Stauber M, Muller R. Micro-computed tomography: a method for the non-destructive evaluation of the three-dimensional structure of biological specimens. Methods Mol Biol. 2008;455:273-292.*)

accomplished by a low-pass filter, but this essentially blurs the image. Edge enhancement requires a high-pass filter, yet this may result in increased noise. Generally, a Gaussian filter does well at balancing these competing objectives, is easy to implement, and is fast, even for large data sets (Fig. 3). It is perhaps the most commonly used filter, but other options such as median filtering also provide good results. Alternatively, examples of edge-preserving filters include the anisotropic diffusion filter and the Laplace-Hamming filter. The rule of thumb is to apply a minimum amount of filtering to avoid degrading the μCT data. For example, too much Gaussian filtration will result in a blurred image that limits the ability to extract bone microarchitecture. A filter always should be applied prior to structural extraction, and it is important that all parameters used to define the filter be reported. For a Gaussian filter, the key parameters are the size of the discrete Gaussian kernel (window) and the standard deviation (σ). Often a support of one or two voxels (eg, $3 \times 3 \times 3$ or $5 \times 5 \times 5$ window, respectively) and a standard deviation of between 0.5 to 2.0 will suffice depending on noise and voxel size, but each application will have different requirements.

Segmentation

The segmentation process is a critical step in the analysis and generally involves separating the mineralized and nonmineralized structures for subsequent quantitative analysis. A mistake at this stage of the μCT analysis will have a systematically impact on all subsequent results. It is essential to compare 2D images from the original and segmented images for some (if not all) μCT scans to ensure that the extracted bone is a good representation of the actual structure. Failure to do this may lead to errors in interpretation of the morphometric data such that one reports altered trabecular bone volume or connectivity when, in fact, the apparent changes are an artifact owing to inaccurate segmentation.

An important issue in segmentation relates to the contouring method employed to define the area in each slice to be included for segmentation and subsequent morphology measurements. The easiest approach is to create a constant circular or rectangular area that captures all the bone of interest. However, this approach does not allow separation of cortical and trabecular bone, and the extra space included around the exterior of the bone structure precludes accurate calculation of bone volume fraction (BV/TV) and other morphologic parameters. More precise contouring for specific cortical and trabecular bone regions therefore is typically warranted and can be achieved manually on a slice-by-slice basis or using automated algorithms.[53,54] There are several approaches to delineating the trabecular region, such as a uniform ROI, an irregular anatomic contour adjacent to the endocortical surface, or an irregular anatomic contour a few pixels away from the endocortical boundary (Fig. 4). The trabecular bone volume of a region whose contour is drawn directly adjacent to the

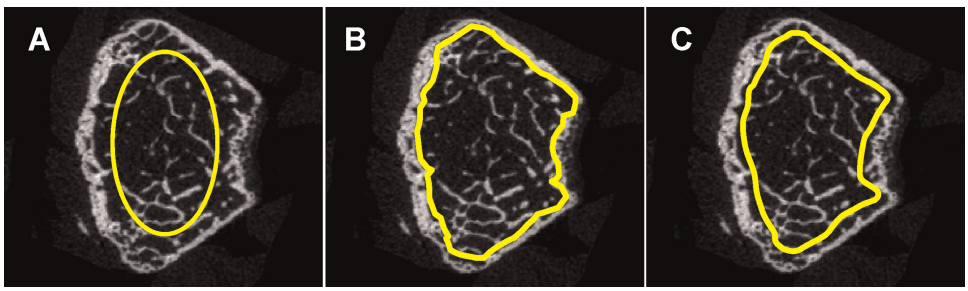

Fig. 4. Contouring methods used to delineate the trabecular bone region. The figure shows three different approaches for identifying the trabecular bone region of interest: (*A*) a regular, uniformly shaped region of interest, (*B*) an irregular, anatomic region of interest adjacent to the endocortical boundary, drawn using an automated algorithm,[53] and (*C*) an irregular, anatomic region of interest drawn manually a few voxels away from the endocortical surface. Images acquired at 70 kVp, 114 mA, 200-ms integration time. (*Images courtesy of Rajaram Manoharan, Beth Israel Deaconess Medical Center.*)

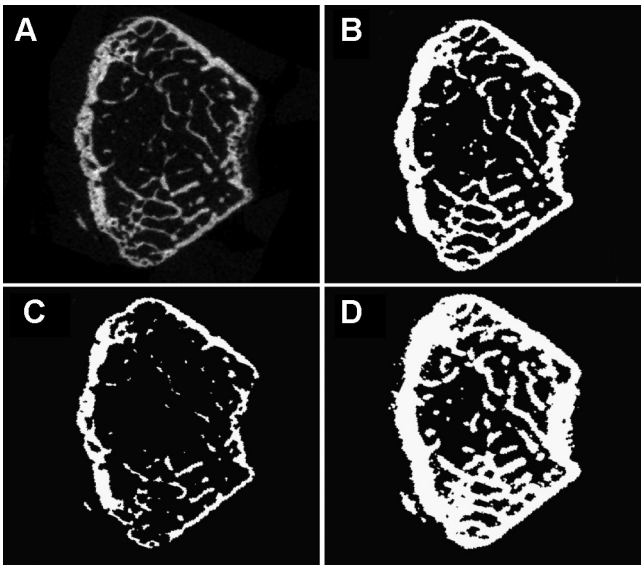

Fig. 5. Effect of different thresholds on image segmentation. (*A*) Original, unsegmented image of mouse distal femur. (*B*) Correctly segmented image showing reasonable binarization of bone structure. (*C*) Image segmented with too high a threshold such that key bone structures are missing and/or thinned relative to the original, unsegmented image. (*D*) Image segmented with too low a threshold such that bone structures appear too thick relative to the original, unsegmented image. Proper segmentation requires visual inspection and comparison of 2D and 3D binarized images with original gray-scale image. Images acquired at 70 kVp, 114 mA, and 200-ms integration time. (*Images courtesy of Rajaram Manoharan, Beth Israel Deaconess Medical Center.*)

endocortical boundary generally will be higher than that of a similar contour drawn a few pixels away from the endocortical surface. Thus, since each of these contouring approaches will lead to different results, it is essential to use the same method in all specimens that are being compared. Furthermore, one must describe the method (manual versus automated) used to delineate the trabecular and cortical bone regions.

Once the region to be analyzed has been identified (or contoured), there are several options for segmentation, all of which have the general goal of extracting a "physiologically and anatomically accurate" representation of the bone tissue (ie, similar to histology).[55] The simplest approach is to use a global threshold that extracts all voxels from the μCT data exceeding a given CT value (density). The advantage of using a global threshold is that it is efficient and requires setting only one parameter. In practice, the threshold is often set using either a fixed CT value or a percent of the CT-value range. To promote comparability across scanners, the equivalent density in milligrams per cubic centimeter of HA should be reported when available. In most studies, using a single global threshold for all scans is possible, and it ensures that differences between study groups are due to experimental effects rather than image-processing effects. Yet there is no consensus on a threshold that should be used for all studies, and extreme care must be taken when selecting a threshold in studies where bone mineralization may not be constant for all groups (ie, during growth and development or fracture healing) or when there are extreme ranges of bone volume fraction among groups,[56,57] in which case a single global threshold may not be adequate. Thus, in some cases, it is necessary to use more sophisticated segmentation tools, including specimen-specific thresholds[58,59] and/or the powerful class of local segmentation methods, where the inclusion of each voxel is based on its local neighborhood. Examples include using the local neighborhood histogram to account for image inhomogeneities owing to beam hardening[60] or using the magnitude of the local image gradient (Sobel operator) to identify bone marrow edges for limited resolution in in vivo images.[6] The increased complexity of these segmentation routines merits caution because they normally require setting a number of parameters, and it is possible that the segmentation process interacts with the experimental treatment effects (eg, changes in tissue density). No matter what segmentation routine is applied, slice-wise 2D comparisons between the original and segmented scan must be performed to ensure accuracy of the segmentation (Fig. 5). If a study design requires the analysis of both cortical and cancellous bone at the same site (eg, vertebral body), then it may be preferable to segment the two tissue types and threshold the volumes separately to delineate bone from non-bone.[61] In any case, a detailed description of the filtration parameters and of the method used to achieve segmentation must be reported to allow proper interpretation and reproduction of μCT data.

In summary, the second step in generating reliable bone morphometry data using μCT is the image processing that occurs after image acquisition, specifically image filtration and segmentation. At a minimum, the methods section of a paper should state any algorithms used for image filtration (including key parameters used to define the filter), the approach used for image segmentation, and the method used to delineate the trabecular and cortical bone regions.

Image Analysis: Bone Morphometry and Tissue Mineral Density

This section provides an overview of the most common morphometric indices that can be derived from the 3D images. Different μCT manufacturers provide different software packages for the computation of these indices; however, the algorithms all should be implemented using the references indicated, and the name of the indices and units always should be standardized, as noted in Tables 2 and 3. This section also describes the use of μCT to estimate tissue mineral density.

Trabecular bone morphometry

The standard method of quantitatively describing bone architecture is the calculation of morphometric indices, also referred to as *quantitative morphometry*. In the past, the microarchitectural characteristics of trabecular and cortical bone have been investigated by examining 2D sections of bone biopsies, combined with calculation of morphometric parameters using stereologic methods.[62] Whereas some measurements such as BV/TV and bone-surface-to-volume ratio (BS/TV) can be obtained directly from 2D images, several key parameters, including trabecular thickness (Tb.Th), trabecular separation (Tb.Sp), and trabecular number (Tb.N), are derived indirectly after assuming a

Table 2. Definition and Description of 3D Outcomes for Trabecular Bone Microarchitecture

Abbreviation	Variable	Description	Standard unit
TV	Total volume	Volume of the entire region of interest	mm^3
BV	Bone volume	Volume of the region segmented as bone	mm^3
BS	Bone surface	Surface of the region segmented as bone	mm^2
BV/TV	**Bone volume fraction**	Ratio of the segmented bone volume to the total volume of the region of interest	%
BS/TV	Bone surface density	Ratio of the segmented bone surface to the total volume of the region of interest	mm^2/mm^3
BS/BV	Specific bone surface	Ratio of the segmented bone surface to the segmented bone volume	mm^2/mm^3
Conn.D	Connectivity density	A measure of the degree of connectivity of trabeculae normalized by TV	$1/mm^3$
SMI	Structure model index	An indicator of the stucture of trabeculae; SMI will be 0 for parallel plates and 3 for cylindrical rods[72]	
Tb.N	**Trabecular number**	Measure of the average number of trabeculae per unit length	1/mm
Tb.Th	**Trabecular thickness**	Mean thickness of trabeculae, assessed using direct 3D methods	mm
Tb.Sp	**Trabecular separation**	Mean distance between trabeculae, assessed using direct 3D methods	mm
Tb.Th.SD	Standard deviation of trabecular thickness	Measure of the homogeneity of trabecular thickness, assessed using direct 3D methods	mm
Tb.Sp.SD	Standard deviation of trabecular separation	Measure of the homogeneity of trabecular separation, assessed using direct 3D methods	mm
DA	Degree of anisotropy	1 = isotropic, >1 = anisotropic by definition; DA = length of longest divided by shortest mean intercept length vector	[a]
MIL	Mean intercept length	Measurements of structural anisotropy	[a]

Note: Variables in bold are the minimal set of variables that should be reported when describing trebecular bone morphology.
[a]Dimensionless variable.

Table 3. Definition and Description of Outcomes for Cortical Bone Morphology

Abbreviation	Variable description	Standard unit
Tt.Ar	Total cross-sectional area inside the periosteal envelope	mm^2
Ct.Ar	Cortical bone area = cortical volume (Ct.V) ÷ (number of slices × slice thickness)	mm^2
Ma.Ar	Medullary (or marrow) area	mm^2
Ct.Ar/Tt.Ar	Cortical area fraction	%
Ct.Th	Average cortical thickness	mm
Ps.Pm	Periosteal perimeter	mm
Ec.Pm	Endocortical perimeter	mm
I_{ap}	Moment of inertia about the anteroposterior axis	mm^4
I_{ml}	Moment of inertia about the mediolateral axis	mm^4
I_{max}	Maximum moment of inertia	mm^4
I_{min}	Minimum moment of inertia	mm^4
J	Polar moment of inertia	mm^4
Ct.Po	Cortical porosity: In a given cortical region, the volume of pores (Po.V, mm^3) ÷ total volume of cortical bone compartment (Ct.V, mm^3)	%
Po.N	Pore number	n
Po.V	Total pore volume	mm^3
AvgPo.V	Average pore volume = Po.V ÷ Po.N	mm^3
Po.V.SD	Standard deviation of pore volume	mm^3
Po.Dn	Pore density = pore number (Po.N, n) ÷ total volume of cortical bone compartment Ct.V (mm^3)	mm^{-3}

Note: Variables in bold are the minimal set of variables that should be reported when describing cortical bone morphology.

fixed-structure model such as a rodlike or platelike structure.[1] These highly idealized models can be considered as two ends of a spectrum, where the real architecture is a mixture of both rods and plates, with the precise composition differing according to skeletal site, disease state, treatment, and age. Thus the correlations among Tb.Th, Tb.Sp, and Tb.N measurements made using 2D methods that require assumptions about the underlying structure and 3D model-independent measurements of these parameters are only modest and vary with skeletal site.[63] Hence deviations in trabecular structure from the assumed plate or rod models will lead to unpredictable errors in the indirectly derived parameters. For this reason, and to take full advantage of the volumetric measurements, it is recommended that 3D model-independent algorithms be used for computing trabecular bone microarchitecture from μCT images.[15,63]

The basic morphometric indices include the measurement of bone volume (BV) and the total volume of interest (TV).[1] These indices can be derived from either a simple voxel-counting method or a more advanced volume-rendering method, also referred to as *volumetric marching cubes* (VOMACs),[64] where the latter method may be more accurate for small or very complex structures. The ratio of these two measures is termed *bone volume fraction* (BV/TV). Another basic measure is the bone surface (BS), which is conventionally computed by triangulation of the object surface using a marching-cubes algorithm.[65] The bone surface density (BS/TV) and specific bone surface (BS/BV) then can be derived easily by dividing the total volume or bone volume, respectively.

As noted earlier, mean trabecular thickness (Tb.Th), mean trabecular separation (Tb.Sp), and mean trabecular number (Tb.N) all should be based on 3D calculations, namely, a sphere-fitting method, where for thickness measurement the spheres are fitted to the object and for separation the spheres are fitted to the background[14] (Fig. 6). The basic approach is to determine the diameter of the largest possible sphere that can be fitted through each voxel that is completely contained within the object (or background) and then to average these diameters. This approach yields a reasonable average thickness of the structure or the background, where the latter reflects the mean trabecular separation. The mean trabecular number is computed as the inverse of the mean distance between the mid-axes of the structure, which are derived via the distance-transformation method.[66] An advantage of this approach to computing trabecular morphometry is that not only mean values but also the variation of those measures are calculated and expressed by the standard deviation.

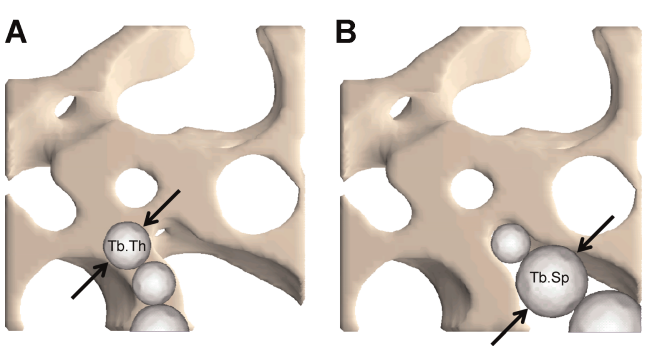

Fig. 6. Schematic representation of algorithm used for direct 3D method for calculating trabecular thickness (*A*) and separation (*B*). 3D distances are computed by fitting spheres inside the structure (ie, to assess average trabecular thickness) or inside the background (marrow space, ie, to assess average trabecular separation). The average diameter of the spheres represents the object thickness, and the standard deviation of the diameter represents the variability in the object thickness. (*Image courtesy of Andres Laib, PhD, Scanco Medical AG.*)

Several studies show that the degree of anisotropy (ie, a description of how the structural elements are oriented), together with bone volume fraction, may explain a significant part of the mechanical properties of a 3D structure. Therefore, several methods to estimate the anisotropy of trabecular bone have been proposed, including those based on mean intercept length (MIL),[67] volume orientation (VO),[68] star volume distribution (SVD),[69] and star length distribution (SLD). These and other measures of architectural anisotropy are reviewed in detail elsewhere.[70]

An index termed *connectivity* (Conn) was developed to characterize the redundancy of trabecular connections. Connectivity is derived from the Euler number,[71] which is a fundamental topologic measure counting the number of objects, the number of marrow cavities fully surrounded by bone, and the number of connections that must be broken to split the structure in two parts. Since the connectivity depends on structure size, it is more appropriate to present this index as a density [connectivity density (Conn.D)] by dividing it by the total volume.[71] To estimate the plate- versus rod-like characteristic of the trabecular bone structure, an index called the *structure model index* (SMI) was developed.[72] This index was designed to be 0 for perfect plates, 3 for perfect rods, and 4 for perfect spheres. However, although this index was designed to yield values in the range of 0 to 4, it may happen that values outside this range occur at very high or very low values of bone volume fraction, and interpretation of these values is difficult. An alternative approach to describing the structure quantifies the actual number of rods and plates within a bone structure.[73]

Cortical bone morphometry

Although a volume of interest is imaged, some aspects of cortical bone morphometry are customarily expressed using area measurements—such as total cross-sectional area (Tt.Ar, mm^2), marrow area (Ma.Ar, mm^2), and cortical bone area (Ct.Ar, mm^2). Using average cross-sectional geometry measurements rather than volume measurements allows comparison across studies when different sized volumes of interest are scanned. To compute average cross-sectional area measurements, the volume of interest (ie, a cylinder) is divided by the number of slices and voxel height (ie, Tt.Ar = Tt.V /(no. of slices × voxel height). Other key parameters for cortical bone include the periosteal and endosteal perimeters (Ps.Pm and Ec.Pm); maximum (I_{max}), minimum (I_{min}), and polar (J) area moments of inertia and/or

[1]Note that our definition of TV as total volume differs from that of the histomorphometry nomenclature guidelines by Parfitt and colleagues (1987),[1] where TV represents tissue volume.

anatomically based moments of inertia for bending about the anteroposteror or mediolateral axes (I_{ap} and I_{ml}, respectively); cortical bone area fraction (Ct.Ar/Tt.Ar, %); and cortical thickness (Ct.Th, μm), where it is recommended that cortical thickness be computed using distance-transform methods.[14] If image resolution is sufficient (ie, pores can be resolved), one also may report cortical porosity (Ct.Po, as Po.V/Ct.V, %), total pore volume (Po.V, mm^3), pore number (Po.N, #), average pore volume (Po.V/Po.N, mm^3), the standard deviation of the pore volume (Po.V.SD, mm^3), and pore density (Po.N/Ct.V, mm^{-3}).

Bone and tissue mineral density

Although μCT has been used primarily to generate information about bone structure, it also can be used to estimate tissue mineral density (TMD). TMD differs from bone mineral density (BMD) in that TMD is calculated from the average attenuation value of the bone tissue only and does not include attenuation values from non-bone voxels, as is done for BMD (whether volumetric or areal). The linear attenuation coefficient measured by μCT, which can be converted to physical density (mg/cm^3 of HA), depends on the physical density and electron density of bone. Because both the amount of mineralized tissue and the degree of mineralization vary among bones, genotype, or times during growth and aging, μCT provides a means to incorporate a measure of mineralization into a study design that is rapid and nondestructive compared with traditional methods for assessing mineralization, such as quantitative microradiography, backscattered electron microscopy, or ash content. However, as previously discussed, the degree of X-ray attenuation is highly dependent on the X-ray energies employed and thus is subject to artifacts attributable to the scanner hardware, specimen size, and specimen tissue density.[17,74] For a polychromatic X-ray source, which pertains to the vast majority of μCT systems, there are several potential sources of artifacts that can alter attenuation values and therefore TMD measurements, including beam hardening, partial-volume effects, photon starvation, photon scatter, and undersampling. Beam-hardening artifacts can be reduced by placing aluminum or copper filters in the beam path to remove the low-energy X-rays and/or by use of beam-hardening correction algorithms.[17] Attenuation artifacts can be reduced by using an aluminum or copper/aluminum filter, a beam flattener, and scanning a full 360 degrees.[75] Scanning for a full 360 degrees appears particularly important for reducing artifacts when multiple samples are scanned simultaneously.

However, despite these approaches for reducing errors in TMD measurements, it is important to recognize that significant errors in TMD measurements can occur when using a polychromatic X-ray source.[17,43,74,76] Under some circumstances, errors are negligible, but under different experimental conditions, the errors can be significant and can compromise the data integrity and interpretation of findings. Investigators must be vigilant in identifying possible errors in TMD that may be associated with their particular experimental conditions, and results must be interpreted with caution. Generally, there is better confidence of comparisons within studies than between studies.

To improve the accuracy of the measurements, some manufacturers use a partial-volume suppression technique in which a fixed number of surface voxels are discarded at the bone–soft tissue interface. Users should know whether their system employs this approach because it will influence the minimum number of voxels that should be included within a structure for reasonable TMD measurements. For example, if two surface voxels are discarded (on each surface), then the mean thickness of the structure must be at least 5 voxels; otherwise, there is no meaningful volume left to determine TMD. Generally, for mouse bones, TMD measurements using standard desktop μCT systems with approximately 10-μm voxel size are possible for diaphyseal cortical bone but are not appropriate for individual trabeculae or for the thin cortex found in metaphyseal regions. New developments in μCT imaging that allow higher-resolution images (approximately 1-μm voxel size) may allow assessment of TMD in mouse trabeculae. In larger animal or human specimens, TMD measurements may be possible for trabecular bone if the resolution is good enough (ie, at least 3 voxels located within the trabeculae). TMD should be reported in units of grams per cubic centimeter or, if an HA phantom is used for calibration, in units of milligrams of HA per cubic centimeter. One must report the method(s) used to reduce beam hardening (ie, hardware, software, or both), the method and frequency at which calibration is performed, and whether partial-volume suppression was employed.

Reporting Results

Reporting quantitative morphometry data

Clearly, the decision on which morphometric indices should be reported depends largely on the research question. Here we propose a minimal set of parameters that should be reported for the characterization of both cortical and trabecular bone in rodents. In long bones, it is recommended to focus on the femur because there is already a relatively large number of studies reporting results for the femur, and values for the accuracy and reproducibility of these measures have been assessed for murine femurs.[7,77] Also, both trabecular and cortical parameters can be evaluated from the distal metaphysis and mid-diaphysis, respectively. The tibia is also acceptable for trabecular bone measurements at the proximal metaphysis and cortical bone measurements at the diaphysis.

The other recommended standard site is the vertebral body, which traditionally has been used for trabecular bone measurements, but it also can be used for cortical bone measurements.[78,79] It is recommended to use lumbar rather than thoracic or caudal spinal segments because the volume of the lumbar vertebral bodies is the greatest, and therefore, more bone is sampled.

The minimal set of variables that should be reported for trabecular regions includes bone volume fraction (BV/TV), trabecular thickness (Tb.Th), trabecular separation (Tb.Sp), and trabecular number (Tb.N) because these can be found in most publications and also can be compared to some extent with classical histomorphometric variables. Depending on the research question, additional variables, such as the structure model index (SMI), connectivity density (Conn.D), degree of anisotropy (DA), and many others, can be reported, but typically only

variables that are critically discussed in the paper should be reported to avoid a long list of variables that are not put into perspective.

The minimal set of variables that should be reported for cortical regions includes total cross-sectional area (Tt.Ar), cortical bone area (Ct.Ar), cortical thickness (Ct.Th), and cortical bone fraction (Ct.Ar/Tt.Ar). Area moments of inertia, cortical porosity, pore morphology, tissue mineral density, and other measurements also may be of interest depending on the research question and ability of the imaging approach to assess these variables accurately.

Presentation of images

In addition to reporting the results from quantitative morphometry, investigators may wish to include some images to assist in visualizing the differences among experimental groups and supporting the statistical analysis of the quantitative endpoints. In this case, whenever possible, standard radiologic guidelines for orientation of clinical CT images should be followed for μCT. Also, it is advised that images of the median animal or, alternatively, of the specimen whose value is closest to the group mean, both selected with respect to one predefined morphometric parameter, be presented. In most cases, the selection of the median or mean animal(s) will be based on bone volume or bone volume fraction depending on the site and type of bone. Although 3D reconstructions of the segmented image data can make very stunning pictures, often 2D sections of original grayscale images provide relevant and synergistic information, depending on the research question. In either case, the approach used to select the "representative image" must be described either in the methods or in the figure legend. If images other than the median animals (eg, extremes from each group) are used, then it must be clearly specified in the methods and/or the figure legends.

Quality Control

To yield the highest-quality images and most accurate results from a μCT scan, steps should be taken to ensure that the system is working properly and that image data are not distorted by scanning artifacts. Users should follow manufacturer's instructions for quality control that are specific to their μCT scanning system.

Phantom Calibration

If results from a μCT scan are to be used to report the density of a sample, it is necessary that the μCT system be calibrated properly using phantom samples of known density, which are in the range of densities expected for the samples to be measured. Many manufacturers provide phantoms that should be measured on a regular basis (daily or weekly) to ensure accurate density readings. Ideally, the thickness of the phantom rod should approximate the thickness of the object to be measured. If the scanner is not calibrated regularly using known density phantoms, then the results of the scan should be reported in terms of pixel brightness (Houndsfield units or linear attenuation coefficient) rather than density (mg HA/cm^3).

Inspection of images: Common artifacts

After scanning, images should be carefully inspected visually. Several scanning artifacts that occur commonly and can strongly affect morphology and density outcomes are readily apparent by visual inspection.[52]

Ring artifact: Occasionally, minor problems such as a defective pixel on the CCD, a defect in the scintillator that converts X-rays to visible light, or dust on the detector system will create an artifact that looks like rings or half rings around the rotation center of the reconstructed image (Fig. 7). Cleaning the system sometimes can eliminate this artifact. For defective pixels, some systems have the ability to replace the pixel electronically using an average of neighboring pixels. Although the data at the defective pixel are lost, averaging will effectively remove the ring artifact.

Metal artifact: Materials with very high linear attenuation coefficients (such as metals) may cause total absorption of the X-ray beam, yielding star-shaped artifacts in the reconstructed images (Fig. 7). This effect can be prevented only by excluding the high-absorbing materials from the scan. Metals such as steel can be replaced by aluminum or titanium, which have much lower linear attenuation coefficients and should not cause this type of artifact.

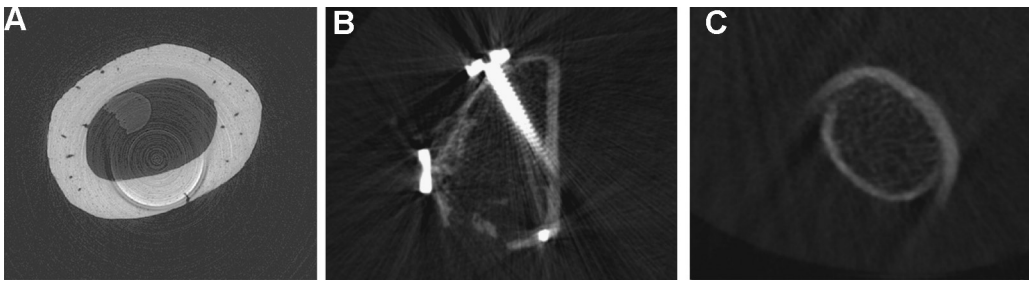

Fig. 7. Examples of common scanning artifacts: (*A*) ring artifact; (*B*) metal artifact; and (*C*) motion artifact. The ring artifact in this image was caused by a defect of the scintillator that converts X-ray to visible light. The screw in panel *B* absorbs much radiation, which results in star-shaped artifacts as well as distortions of the image in its neighborhood. Panel C shows the ulna of a patient measurement in which the patient moved the arm during measurement. For this reason, the cortex is not a closed ring but rather composed of two half rings that go along with two tails. (*Images reproduced with permission from Stauber M, Muller R. Micro-computed tomography: a method for the non-destructive evaluation of the three-dimensional structure of biological specimens. Methods Mol Biol. 2008;455:273-292.*)

Motion artifact: During scanning, a sample typically is rotated relative to the radiation source (or reversed in the case of in vivo scanners) to obtain X-ray projections from multiple angles. If the object moves within the scanning tube during this rotation, the projections will not fit together properly during reconstruction, resulting in distortion of the object (Fig. 7). For this reason, it is important to stabilize the sample properly so that no extraneous motion will occur during scanning. Misalignment of the center of rotation also can appear to be a motion artifact. In this case, a phantom measurement (which presumably would have no possibility for motion) should be performed to distinguish between the two possible sources for the artifact.

Special Considerations for Murine Imaging Studies

There are a number of special considerations for achieving high-quality bone morphometry data in the mouse skeleton. Among the key challenges is the small size of the bones and structures of interest, such as trabecular thickness or cortical thickness in the metaphyseal regions or vertebral body—particularly in young animals. Thus the choice of voxel size is critical for reliable measurements.

Skeletal sites of interest also must be selected carefully depending on the specific research question. For trabecular bone analysis of mice or rats, the sites investigated most often are the proximal tibia, distal femur, and vertebral body. It may be desirable to analyze more than one skeletal site, particularly an appendicular and axial site, because heterogeneity among skeletal sites has been reported previously,[56,80,81] although the optimal study design and choice of μCT analyses will depend on the research question. When considering the research question, it should be noted that age-related trabecular bone loss begins at a relatively young age in the metaphyseal regions of the long bones and continues into old age such that bone volume fraction can be as low as a few percent in aged animals.[56] This very low bone volume makes it challenging to detect differences between groups and makes it particularly difficult to detect bone loss or inhibition of bone loss in an adult animal and/or skeletal region that has already undergone significant bone loss. In comparison, in the vertebral body, age-related trabecular bone loss begins at a later age and is not as dramatic.[56] Another caveat with the mouse is that certain strains are known to have very few trabeculae at certain skeletal sites (eg, proximal tibia of C57BL/6J), particularly in older animals,[56] and this very low number of trabeculae may lead to exaggerated conclusions (eg, an increase from one trabecula to two would appear to be a relatively large change). Moreover, one must be very cautious in interpreting certain morphometric data, particularly connectivity and anisotropy, when few trabeculae are included in the ROI.

Selecting the volume of interest at a particular skeletal site is an important issue. In mice especially, trabecular bone in the metaphyseal region is largely confined to a few millimeters adjacent to the metaphyseal growth plate. Extending a volume of interest beyond this region would include more "empty space." thereby reducing the mean values for BV/TV at that skeletal site and possibly masking relevant differences between study groups (Fig. 8).

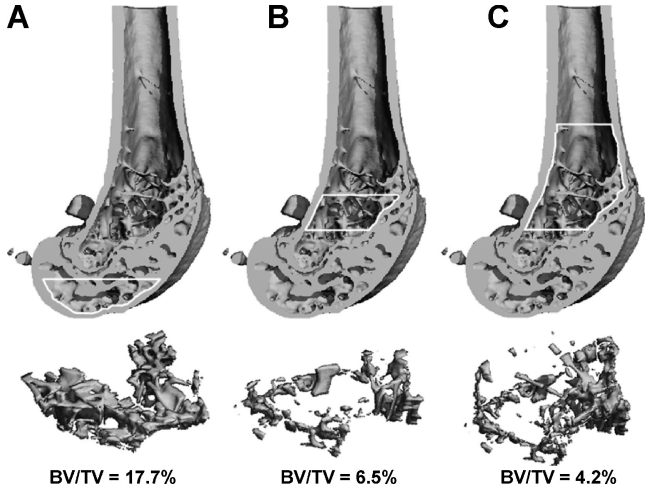

Fig. 8. Influence of the volume of interest on trabecular BV/TV at the distal femur of a 24-week-old female C57BL/6 mouse. Evaluation of epiphyseal trabecular bone (*A*) typically will yield a much higher BV/TV than evaluation of metaphyseal trabecular bone (*B*, *C*). Likewise, a volume of interest limited to the metaphyseal trabecular bone close to the growth plate (*B*) will yield a higher BV/TV than a larger volume of interest that includes a large amount of "empty space" in the diaphysis that contains few trabeculae (*C*). (*Images reproduced with permission from Christiansen BA and Bouxsein ML. Assessment of bone mass and microarchitecture in rodents. In Rosen CJ, ed. Primer on Metabolic Bone Diseases and Disorders of Mineral Metabolism, 7th ed. Washington, DC: American Society for Bone and Mineral Research; 2008:38–44.*)

Additional Current and Future Uses for μCT Imaging of Small Animals

This section reviews a few of the nonstandard uses of μCT for imaging studies, some of which are likely to become more prominent and therefore deserve mention, as well as discussing the use of synchrotron-based imaging systems. In particular, in vivo high-resolution imaging is likely to become a standard method for small animal studies and is thus discussed below. Radiopaque contrast agents have been employed to provide enhanced imaging capabilities in several different scenarios, including assessment of microdamage,[82] vascular morphology,[35,83–85] and cartilage degradation.[40,42] Principles from preceding sections regarding image acquisition, analysis, and reporting are relevant here, although, wherever possible, we point out unique considerations for these nonstandard uses of μCT imaging.

In vivo μCT

In vivo μCT provides the high resolution of μCT while allowing for longitudinal studies of bone morphology. In vivo μCT thus is an ideal strategy for tracking bone changes that occur on a time scale of weeks or months, such as bone loss associated with disuse or ovariectomy or increased bone mass owing to pharmacologic or mechanical intervention. By registering 3D images against images from previous time points, it is possible to determine the precise locations of bone formation or resorption[86–88] (Fig. 9). The ability to perform longitudinal assessments of bone microstructure has the potential to reduce the number

Fig. 9. In vivo longitudinal μCT images of the proximal tibia of a 30-week-old Wistar rat at baseline and then 2 and 4 weeks after ovariectomy. Note the marked deterioration of trabecular bone in the metaphysis, particularly adjacent to the growth plate, in comparison with little change in the epiphysis. (*Images courtesy of J. E. M. Brouwers, Eindhoven University of Technology, and reproduced with permission from Christiansen BA and Bouxsein ML. Assessment of bone mass and microarchitecture in rodents. In Rosen CJ, ed. Primer on Metabolic Bone Diseases and Disorders of Mineral Metabolism, 7th ed. Washington, DC: American Society for Bone and Mineral Research; 2008:38–44.*)

of animals needed in a given study and provide novel information about skeletal development, adaptation, repair, and response to disease or therapeutic interventions. For example, in vivo μCT has been used to follow the rapid trabecular bone loss in rats in the weeks immediately following ovariectomy[87,89] and was able to discern significant "irreversible" reductions in trabecular connectivity after only 2 weeks.[89] In vivo μCT also has been used to study the effects of aging,[90] disuse,[91–93] whole-body vibration,[94] and pharmacologic treatments.[95,96] In addition to measuring bone morphology, Judex and colleagues[97] have demonstrated that in vivo μCT can be used to assess total-body fat and the size of regional fat deposits in mice.

Despite the clear advantages of in vivo μCT, there are also several issues to consider. First, there are concerns about the amount of ionizing radiation delivered during the in vivo μCT scan, particularly when animals are scanned multiple times throughout an experimental period. This radiation may introduce unwanted effects on the tissues or processes of interest or on the animals in general. Young, growing animals and proliferative biologic processes, such as fracture healing or tumor growth, may be particularly susceptible to radiation exposure. The radiation exposure reported by Waarsing and colleagues,[86] namely, 0.4 Gy for a single 20-minute μCT scan (10-μm voxel size) of a rat hind limb, is not predicted to have significant deleterious effects on bone cells,[98] but the effect of multiple exposures needs additional investigation. Klinck and colleagues[99] performed weekly in vivo μCT scans of the proximal tibia of ovariectomized and sham-operated rats beginning at 12 weeks of age. With an estimated 0.5 Gy exposure per scan, they found no observable effects of radiation on the animals' overall health, but trabecular bone volume was 8% to 20% lower in the irradiated limbs than in the contralateral nonirradiated limbs. Importantly, radiation effects may be greater in some tissues than in others and at some ages than at others. In particular, tumors are likely to be highly susceptible to the effects of radiation, and thus there is a high likelihood that studies of tumor initiation and progression could be adversely affected by exposure to radiation from in vivo μCT measurements. It is clear that additional studies are needed to determine the potential effects of repeated in vivo μCT scans in a variety of experimental models. Furthermore, current observations provide strong rationale for the inclusion of measurements of an internal nonirradiated control limb in the study design whenever possible. Investigators should report the dose rate (in mGy/min) as measured by an ionization chamber with appropriate shielding by a tissue-equivalent plastic.

A second potential limitation of in vivo μCT imaging relates to possible movement artifacts that may be introduced owing to the animal's breathing. This is a negligible concern when scanning peripheral limbs, but motion should be taken into account when scanning the axial skeleton. The final issue associated with in vivo imaging is concern over the ability to monitor changes in individual bone structures accurately and precisely over time. Although theoretically possible and highly intriguing, accomplishing this requires accurate registration of images acquired at different time points, an area of active research.[87]

Contrast-enhanced μCT imaging of vascularization

Vascular imaging is highly desirable given that the processes of angiogenesis and osteogenesis are intimately linked during bone development, growth, remodeling, and repair. Traditional histologic approaches to vascular imaging and analysis have significant limitations that may be overcome with the 3D high-resolution quantitative capabilities of μCT. Unfortunately, the attenuation of hydrated soft tissues such as blood vessels is typically too low to detect directly via μCT imaging. However, vascular structures can be visualized and quantified using 3D μCT analysis combined with a perfused contrast agent.

Using a murine hind limb ischemia model, Duvall and colleagues demonstrated the utility of contrast-enhanced μCT analysis to quantify 3D vascular network morphologic parameters, including vessel volume, thickness, number, connectivity, and degree of anisotropy.[84,85] Briefly, the technique involves perfusion of a radiodense silicone rubber contrast agent containing lead chromate (Microfil MV-122, Flow Tech, Carver, MA, USA) through the vasculature at the time of euthanasia. Other types of contrast agents also may be used, but it is important to assess the ability of each agent to provide reproducible and stable perfusion throughout the vasculature and homogeneous attenuation that

allows segmentation from surrounding tissues. Applications of the vascular μCT imaging technique have included studies on response to ischemic injury,[84,85] phenotypic characterization of tissue repair and remodeling,[85] therapeutic angiogenesis,[83] postnatal development and growth,[100,101] cerebral circulation,[102] vascular biomechanics and disease,[103] fracture healing,[35] and tissue engineering[104,105] (Fig. 10).

Segmentation and image resolution affect the ability of μCT imaging to detect vascular structures of different sizes.[84] Samples can be demineralized prior to scanning to facilitate segmentation of vascularization from bone. If analysis of bone and vasculature are desired, an effective approach is to combine in vivo μCT imaging of bone with postmortem imaging of vasculature following demineralization. Selection of the optimal voxel size should be based on the intended application. Potential limitations of this technique include incomplete perfusion of the vasculature. Artifacts also can result from perfusing at too high of a pressure, resulting in leakage of the contrast agent from the vessels. The presence of bulbous structures in reconstructed images that do not resemble vascular structures is clear evidence of contrast agent leakage.

Other limitations of the vascular imaging method just described are that it cannot provide longitudinal assessment in vivo and has been applied primarily in small-animal models. In vivo contrast agents are increasingly becoming available, although detection and segmentation remain a challenge.[106] Finally, μCT does not provide a direct measure of vascular function, although μCT-based measures of vascular growth following ischemic injury correspond well with laser-Doppler assessment of limb perfusion and functional testing of muscle.[85]

Contrast-enhanced μCT imaging of cartilage

MRI is the standard method for clinical joint imaging but has insufficient resolution for analyzing articular cartilage in mice and rats. A high-resolution 3D imaging method would be useful for evaluation of joint changes in small-animal osteoarthritis models or cartilage matrix synthesis within biomaterials. Palmer and colleagues introduced a technique to detect and quantify proteoglycan (PG) content by imaging the equilibrium partitioning of an ionic contrast agent via μCT (EPIC-μCT).[40] The principle of the technique relies on a negatively charged contrast agent (Hexabrix 320, Mallinckrodt, Hazelwood, MO, USA) equilibrating within cartilaginous tissues at concentrations inversely proportional to the local concentration of negatively charged sulfated glycosaminoglycans (sGAGs). Regions of low PG content thus have relatively higher X-ray attenuation, whereas regions of higher PG content result in reduced contrast agent concentration and therefore reduced image voxel density.

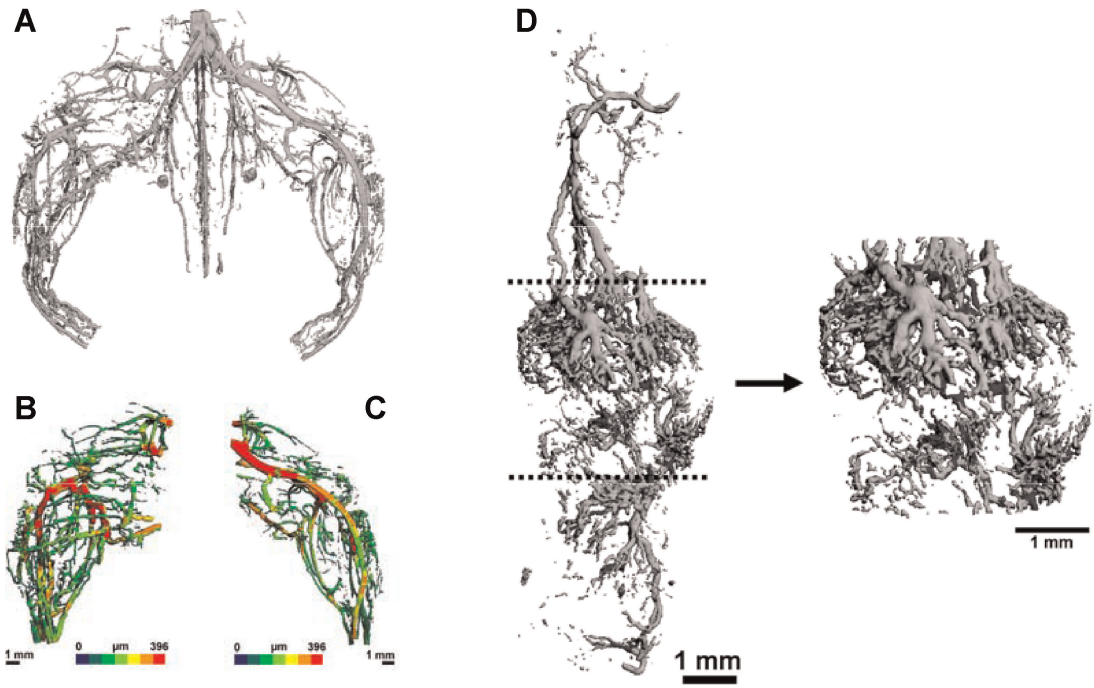

Fig. 10. Representative μCT images of mouse hind limb vasculature following ligation and excision of the femoral artery and vein in the right leg. No surgical procedure was performed on the left leg. Microfil MV-122 lead chromate–based contrast agent was pressure perfused throughout the vasculature to enhance X-ray attenuation, and the images were obtained at the 14-day postoperative time point using a Scanco μCT 40. (*A*) Image from an entire perfused hindlimb scanned at 36-μm voxel size. Images of surgical (*B*) and control (*C*) volumes of interest (36-μm voxel size) have been mapped with color-coded vessel diameter data derived from direct transformation methods. (*D*) A representative vascular μCT image obtained from a mouse femur 14 days after fracture and scanned with a Scanco vivaCT 40 at 10.5-μm voxel size. The vasculature was pressure-perfused with Microfil MV-122, and bone was decalcified prior to scanning. Morphometric parameters were quantified for a standardized callus length, as marked by the dotted lines and depicted in an expanded view to the right. (*Reproduced with permission from Lin ASP, Palmer AW, Duvall CL, et al. Contrast enhanced micro-CT imaging of soft tissues. In Lin Q, Genant HK, Griffith JF, and Leung KS, eds. Advanced Bioimaging Technologies in Assessment of the Quality of Bone and Scaffold Materials. Heidelberg, Germany: Springer-Verlag; 2007:239–256.*)

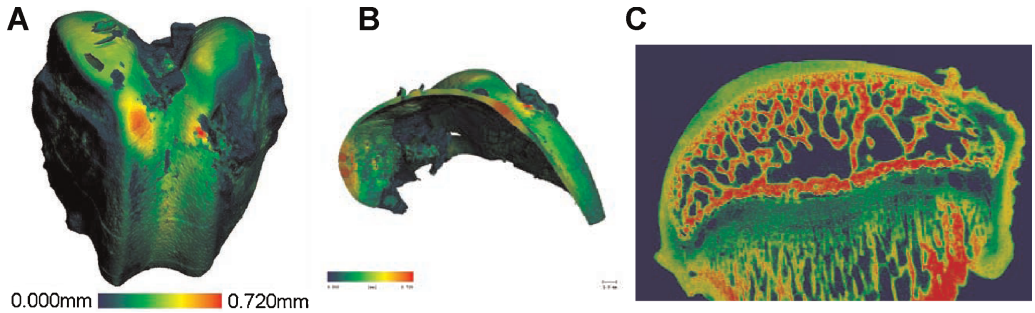

Fig. 11. EPIC-μCT image of intact rabbit distal femur (*A*) and segmented articular cartilage with surface thickness map (*B*). (Reproduced with permission from Palmer AW, Guldberg RE, Levenston ME. Analysis of cartilage matrix fixed charge density and three-dimensional morphology via contrast-enhanced microcomputed tomography. Proc Natl Acad Sci USA. 2006;103:19255-19260.) Articular cartilage is visible and can be segmented from the underlying subchondral bone in a rat joint following equilibration in an ionic contrast agent (*C*)

The ability of EPIC-μCT to nondestructively monitor changes in cartilage composition over time was validated in a bovine articular cartilage explant degradation model by showing a strong linear correlation between voxel attenuation and biochemical measurement of sGAG content.[40] Subsequent studies have validated the ability of the EPIC-μCT technique to quantify changes in the morphology and composition of articular cartilage in a rat knee arthritis model.[41] Importantly, contrast-enhanced regions of cartilage can be segmented from subchondral bone, providing a detailed thickness map of the articular cartilage and the ability to analyze bone and cartilage simultaneously (Fig. 11). Moreover, as long as segmentation can be achieved, it should be possible to combine contrast-agent techniques to analyze mineralized tissues, cartilage, and vasculature. High-resolution 3D images and quantitative morphometric analysis of multiple tissues would be invaluable for studies on development, growth, and repair of musculoskeletal tissues.

Synchrotron radiation μCT (SR-μCT)

In synchrotron radiation (SR)–based μCT (or nano-CT), the polychromatic X-ray source used for standard desktop μCT imaging systems is replaced by a high-photon-flux monochromatic X-ray beam that is extracted from a synchrotron source. The advantages of this approach relative to standard μCT include (1) the use of an X-ray beam with just one energy, eliminating beam-hardening artifacts and allowing for accurate assessment of tissue mineral density,[107] (2) increased spatial resolution (approximately 1 μm and below), and (3) very high SNR.[3,108] The high spatial resolution associated with SR-μCT affords extremely precise assessment of trabecular bone architecture[3] and may be particularly useful for assessment of small-scale bone structures in young animals.[109,110] SR-μCT also has been used recently to investigate genetic variations in the mineral density and ultrastructural properties of murine cortical bone, including the vascular canals and osteocyte lacunae.[111,112] Although studies with SR-μCT generally are performed on excised specimens, Kinney and colleagues[108] used SR-μCT in vivo in the rat proximal tibia to show the early deterioration in trabecular architecture following estrogen deficiency.

Altogether, SR-μCT offers extremely high-resolution imaging of microarchitecture and mineral density in excised bone specimens. The disadvantages of the technique are its limited availability (ie, it requires access to a synchrotron source), relatively small volume of tissue examined, and technical expertise needed to acquire and analyze the measurements.

Summary of Recommendations

We have outlined standardized nomenclature and attempted to provide both general and specific guidelines for the use of μCT imaging to assess bone morphology and density in rodents. Clearly, the specific research questions will dictate the methodology used for any particular experiment. However, the recommendations for standardized nomenclature and reporting of methodology and results provided in these guidelines will allow for more transparent interpretation of results and more robust comparisons across studies. The key recommendations for any publication that uses μCT imaging are summarized as follows:

- With regard to *image acquisition*, the methods section should report the following parameters: scan medium, X-ray tube potential, and voxel size, as well as clear descriptions of the size and location of the volume of interest.
- With regard to *image processing*, the methods section should describe any algorithms used for image filtration and the approach used for image segmentation, including the method used to delineate cortical from trabecular bone regions.
- With regard to *image analysis*, 3D algorithms that do not rely on assumptions about the underlying structure should be used to compute trabecular and cortical bone morphometry whenever possible. Whereas tissue mineral density measurements are possible with μCT systems, significant artifacts can be associated with the use of polychromatic X-ray sources, and therefore, these measurements must be conducted with extreme care and interpreted with caution.
- With regard to *reporting of μCT results*, the minimal set of variables that should be used to describe trabecular bone morphometry include bone volume fraction and trabecular number, thickness, and separation. The minimal set of variables that should be used to describe cortical bone morphometry includes total cross-sectional area, cortical bone area, cortical bone area fraction, and cortical thickness. Other variables also may be appropriate depending on the research question. Standard nomenclature, as outlined in

Tables 2 and 3, should be followed for the reporting of results.

- With regard to *presentation of μCT images*, either 2D or 3D images are appropriate, but the criteria used to select the "representative" image(s) must be described either in the methods section or the figure legend.
- With regard to *quality control*, investigators should follow manufacturer-specific instructions for regular quality control and document that these instructions are followed. All images should be inspected visually to identify possible scanning artifacts.

Disclosures

All the authors state that they have no conflicts of interest.

Acknowledgments

We acknowledge the following individuals (listed alphabetically) who provided helpful comments during the drafting of these guidelines: Mohammed Ahkter, Andrew Burghardt, Robert Fajardo, Claus Glüer, Marc Grynpas, Stefan Judex, Rasesh Kapadia, Andres Laib, Sharmila Majumdar, Michael Ominsky, Phil Salmon, Neil Sharkey, Matthew Silva, Larry Suva, and Aurore Varela, and Laurence Vico. We also thank Rajaram Manoharan of the Center for Advanced Orthopedic Studies at Beth Israel Deaconess Medical Center and Andres Laib of Scanco Medical AG for providing several figures.

References

1. Parfitt A, Drezner M, Glorieux F, Kanis J, Recker R. Bone histomorphometry: standardization of nomenclature, symbols and units. J Bone Miner Res. 1987;2:595–610.
2. Feldkamp LA, Goldstein SA, Parfitt AM, Jesion G, Kleerekoper M. The direct examination of three-dimensional bone architecture in vitro by computed tomography. J Bone Miner Res. 1989;4:3–11.
3. Martin-Badosa E, Amblard D, Nuzzo S, Elmoutaouakkil A, Vico L, Peyrin F. Excised bone structures in mice: imaging at three-dimensional synchrotron radiation micro CT. Radiology. 2003;229:921–928.
4. Kapadia RD, Stroup GB, Badger AM, et al. Applications of micro-CT and MR microscopy to study pre-clinical models of osteoporosis and osteoarthritis. Technol Health Care. 1998;6:361–372.
5. Bonnet N, Laroche N, Vico L, Dolleans E, Courteix D, Benhamou CL. Assessment of trabecular bone microarchitecture by two different X-ray microcomputed tomographs: a comparative study of the rat distal tibia using Skyscan and Scanco devices. Med Phys. 2009;36:1286–1297.
6. Waarsing JH, Day JS, Weinans H. An improved segmentation method for in vivo microCT imaging. J Bone Miner Res. 2004; 19:1640–1650.
7. Alexander J, Bab I, Fish S, et al. Human parathyroid hormone 1-34 reverses bone loss in ovariectomized mice. J Bone Min Res. 2001;16:1665–1673.
8. Barbier A, Martel C, de Vernejoul MC, et al. The visualization and evaluation of bone architecture in the rat using three-dimensional X-ray microcomputed tomography. J Bone Miner Metab. 1999; 17:37–44.
9. Kuhn JL, Goldstein SA, Feldkamp LA, Goulet RW, Jesion G. Evaluation of a microcomputed tomography system to study trabecular bone structure. J Orthop Res. 1990;8:833–842.
10. Müller R, Van Campenhout H, Van Damme B, et al. Morphometric analysis of human bone biopsies: a quantitative structural comparison of histological sections and micro-computed tomography. Bone. 1998;23:59–66.
11. Fanuscu MI, Chang TL. Three-dimensional morphometric analysis of human cadaver bone: microstructural data from maxilla and mandible. Clin Oral Implants Res. 2004;15:213–218.
12. Chappard D, Retailleau-Gaborit N, Legrand E, Basle MF, Audran M. Comparison insight bone measurements by histomorphometry and microCT. J Bone Miner Res. 2005;20:1177–1184.
13. Akhter MP, Lappe JM, Davies KM, Recker RR. Transmenopausal changes in the trabecular bone structure. Bone. 2007;41:111–116.
14. Hildebrand T, Rüegsegger P. A new method for the model independent assessment of thickness in three-dimensional images. J Micros. 1997;185:67–75.
15. Laib A, Hildebrand T, Hauselmann HJ, Ruegsegger P. Ridge number density: a new parameter for in vivo bone structure analysis. Bone. 1997;21:541–546.
16. Hildebrand T, Rüesegger P. Quantification of bone microarchitecture with the structure model index. Comp Meth Biomech Biomed Eng. 1997;1:5–23.
17. Fajardo RJ, Cory E, Patel ND, et al. Specimen size and porosity can introduce error into microCT-based tissue mineral density measurements. Bone. 2009;44:176–184.
18. van Rietbergen B, Majumdar S, Pistoia W, et al. Assessment of cancellous bone mechanical properties from micro-FE models based on micro-CT, pQCT and MR images. Technol Health Care. 1998;6:413–420.
19. Layton MW, Goldstein SA, Goulet RW, Feldkamp LA, Kubinski DJ, Bole GG. Examination of subchondral bone architecture in experimental osteoarthritis by microscopic computed axial tomography. Arthritis Rheum. 1988;31:1400–1405.
20. Hankenson KD, Hormuzdi SG, Meganck JA, Bornstein P. Mice with a disruption of the thrombospondin 3 gene differ in geometric and biomechanical properties of bone and have accelerated development of the femoral head. Mol Cell Biol. 2005;25:5599–5606.
21. Turner CH, Hsieh YF, Muller R, et al. Genetic regulation of cortical and trabecular bone strength and microstructure in inbred strains of mice. J Bone Miner Res. 2000;15:1126–1131.
22. Jepsen KJ, Akkus OJ, Majeska RJ, Nadeau JH. Hierarchical relationship between bone traits and mechanical properties in inbred mice. Mamm Genome. 2003;14:97–104.
23. Bouxsein ML, Myers KS, Shultz KL, Donahue LR, Rosen CJ, Beamer WG. Ovariectomy-induced bone loss varies among inbred strains of mice. J Bone Miner Res. 2005;20:1085–1092.
24. Bonadio J, Jepsen KJ, Mansoura MK, Jaenisch R, Kuhn JL, Goldstein SA. A murine skeletal adaptation that significantly increases cortical bone mechanical properties. Implications for human skeletal fragility. J Clin Invest. 1993;92:1697–1705.
25. Lewis DB, Liggitt HD, Effmann EL, et al. Osteoporosis induced in mice by overproduction of interleukin 4. Proc Natl Acad Sci U S A. 1993;90:11618–11622.
26. Silva MJ, Brodt MD, Uthgenannt BA. Morphological and mechanical properties of caudal vertebrae in the SAMP6 mouse model of senile osteoporosis. Bone. 2004;35:425–431.
27. Laib A, Kumer JL, Majumdar S, Lane NE. The temporal changes of trabecular architecture in ovariectomized rats assessed by MicroCT. Osteoporos Int. 2001;12:936–941.
28. Hopper TA, Wehrli FW, Saha PK, et al. Quantitative microcomputed tomography assessment of intratrabecular, intertrabecular, and

cortical bone architecture in a rat model of severe renal osteodystrophy. J Comput Assist Tomogr. 2007;31:320–328.

29. von Stechow D, Zurakowski D, Pettit AR, et al. Differential transcriptional effects of PTH and estrogen during anabolic bone formation. J Cell Biochem. 2004;93:476–490.
30. Christiansen BA, Silva MJ. The effect of varying magnitudes of whole-body vibration on several skeletal sites in mice. Ann Biomed Eng. 2006;34:1149–1156.
31. Squire M, Donahue LR, Rubin C, Judex S. Genetic variations that regulate bone morphology in the male mouse skeleton do not define its susceptibility to mechanical unloading. Bone. 2004; 35:1353–1360.
32. Uthgenannt BA, Silva MJ. Use of the rat forelimb compression model to create discrete levels of bone damage in vivo. J Biomech. 2007;40:317–324.
33. Naik AA, Xie C, Zuscik MJ, et al. Reduced COX-2 expression in aged mice is associated with impaired fracture healing. J Bone Miner Res. 2009;24:251–264.
34. Gardner MJ, Ricciardi BF, Wright TM, Bostrom MP, van der Meulen MC. Pause insertions during cyclic in vivo loading affect bone healing. Clin Orthop Relat Res. 2008;466:1232–1238.
35. Duvall CL, Taylor WR, Weiss D, Wojtowicz AM, Guldberg RE. Impaired angiogenesis, early callus formation, and late stage remodeling in fracture healing of osteopontin-deficient mice. J Bone Miner Res. 2007;22:286–297.
36. Shen X, Wan C, Ramaswamy G, et al. Prolyl hydroxylase inhibitors increase neoangiogenesis and callus formation following femur fracture in mice. J Orthop Res. 2009;27:1298–1305.
37. Gerstenfeld LC, Sacks DJ, Pelis M, et al. Comparison of effects of the bisphosphonate alendronate versus the RANKL inhibitor denosumab on murine fracture healing. J Bone Miner Res. 2009;24:196–208.
38. Morgan EF, Mason ZD, Chien KB, et al. Micro-computed tomography assessment of fracture healing: relationships among callus structure, composition, and mechanical function. Bone. 2009;44:335–344.
39. Bolland BJ, Kanczler JM, Dunlop DG, Oreffo RO. Development of in vivo muCT evaluation of neovascularisation in tissue engineered bone constructs. Bone. 2008;43:195–202.
40. Palmer AW, Guldberg RE, Levenston ME. Analysis of cartilage matrix fixed charge density and three-dimensional morphology via contrast-enhanced microcomputed tomography. Proc Natl Acad Sci U S A. 2006;103:19255–19260.
41. Xie L, Lin AS, Guldberg RE, Levenston ME. Nondestructive assessment of sGAG content and distribution in normal and degraded rat articular cartilage via EPIC-muCT. Osteoarthritis Cartilage. 2009.
42. Xie L, Lin AS, Levenston ME, Guldberg RE. Quantitative assessment of articular cartilage morphology via EPIC-microCT. Osteoarthritis Cartilage. 2009;17:313–320.
43. Nazarian A, Snyder BD, Zurakowski D, Muller R. Quantitative microcomputed tomography: a non-invasive method to assess equivalent bone mineral density. Bone. 2008;43:302–311.
44. Hsieh J. *Computed tomography: principles, design, artifacts, and recent advances*. Bellingham, WA: SPIE—The International Society for Optical Engineering; 2003.
45. Ritman EL. Micro-computed tomography-current status and developments. Annu Rev Biomed Eng. 2004; 6: 185–208.
46. Rüegsegger P, Müller R. Quantitative computed tomography techniques in the determination of bone density and bone architecture. In: Leondes C, ed. *Medical Imaging Systems Techniques and Applications—Brain and Skeletal Systems*. Singapore: Gordon and Breach Science Publishers; 1997: pp 169–220.
47. Müller R, Koller B, Hildebrand T, Laib A, Gianolini S, Rüegsegger P. Resolution dependence of microstructural properties of cancellous bone based on three-dimensional micro-tomography. Technology and Health Care. 1996;9:1–7.
48. Guldberg RE, Hollister SJ, Charras GT. The accuracy of digital image-based finite element models. J Biomech Eng. 1998;120:289–295.
49. Kalendar W. *Computed Tomography*. Erlangen: Publicis Corporate Publishing; 2005.
50. Harrigan TP, Jasty M, Mann RW, Harris WH. Limitations of the continuum assumption in cancellous bone. J Biomech. 1988; 21:269–275.
51. Fajardo RJ, Muller R. Three-dimensional analysis of nonhuman primate trabecular architecture using micro-computed tomography. Am J Phys Anthropol. 2001;115:327–336.
52. Stauber M, Muller R. Micro-computed tomography: a method for the non-destructive evaluation of the three-dimensional structure of biological specimens. Methods Mol Biol. 2008;455:273–292.
53. Buie HR, Campbell GM, Klinck RJ, MacNeil JA, Boyd SK. Automatic segmentation of cortical and trabecular compartments based on a dual threshold technique for in vivo micro-CT bone analysis. Bone. 2007;41:505–515.
54. Kohler T, Stauber M, Donahue LR, Muller R. Automated compartmental analysis for high-throughput skeletal phenotyping in femora of genetic mouse models. Bone. 2007;41:659–667.
55. Rajagopalan S, Lu L, Yaszemski MJ, Robb RA. Optimal segmentation of microcomputed tomographic images of porous tissue-engineering scaffolds. J Biomed Mater Res A. 2005;75:877–887.
56. Glatt V, Canalis E, Stadmeyer L, Bouxsein ML. Age-related changes in trabecular architecture differ in female and male C57BL/6J mice. J Bone Miner Res. 2007;22:1197–1207.
57. Ominsky MS, Stolina M, Li X, et al. One year of transgenic overexpression of osteoprotegerin in rats suppressed bone resorption and increased vertebral bone volume, density, and strength. J Bone Miner Res. 2009;24:1234–1246.
58. Ridler T, Calvard S. Picture thresholding using an iterative selection method. IEEE Trans on Systems, Man and Cybernetics SMC. 1978; 8:630–632.
59. Meinel L, Fajardo R, Hofmann S, et al. Silk implants for the healing of critical size bone defects. Bone. 2005;37:688–698.
60. Dufresne T. Segmentation techniques for analysis of bone by three-dimensional computed tomographic imaging. Technol Health Care. 1998;6:351–359.
61. Tommasini SM, Hu B, Nadeau JH, Jepsen KJ. Phenotypic integration among trabecular and cortical bone traits establishes mechanical functionality of inbred mouse vertebrae. J Bone Miner Res. 2009; 24:606–620.
62. Parfitt AM, Mathews CH, Villanueva AR, Kleerekoper M, Frame B, Rao DS. Relationships between surface, volume, and thickness of iliac trabecular bone in aging and in osteoporosis. Implications for the microanatomic and cellular mechanisms of bone loss. J Clin Invest. 1983;72:1396–1409.
63. Hildebrand T, Laib A, Muller R, Dequeker J, Ruegsegger P. Direct three-dimensional morphometric analysis of human cancellous bone: microstructural data from spine, femur, iliac crest, and calcaneus. J Bone Miner Res. 1999;14:1167–1174.
64. Muller R, Ruegsegger P. Three-dimensional finite element modelling of non-invasively assessed trabecular bone structures. Med Eng Phys. 1995;17:126–133.
65. Lorensen W, Cline H. Marching cubes: a high resolution 3D surface construction algorithm. Computer Graphics. 1987;21:163–169.

66. Danielson P-E. Euclidean distance mapping. Comp Vision Graph Image Processing. 1980;14:227–248.

67. Whitehouse WJ. The quantitative morphology of anisotropic trabecular bone. J Microsc. 1974;101:153–168.

68. Odgaard A, Jensen EB, Gundersen HJ. Estimation of structural anisotropy based on volume orientation. A new concept. J Microsc. 1990;157:149–162.

69. Cruz-Orive L, Karlsson L, Larsen S, Wainschtein F. Characterizing anisotropy: a new concept. Micron and Microscopica Acta. 1992; 23:75–76.

70. Odgaard A. Three-dimensional methods for quantification of cancellous bone architecture. Bone. 1997;20:315–328.

71. Odgaard A, Gundersen HJ. Quantification of connectivity in cancellous bone, with special emphasis on 3-D reconstructions. Bone. 1993;14:173–182.

72. Hildebrand T, Ruegsegger P. Quantification of Bone Microarchitecture with the Structure Model Index. Comput Methods Biomech Biomed Engin. 1997;1:15–23.

73. Stauber M, Muller R. Volumetric spatial decomposition of trabecular bone into rods and plates--a new method for local bone morphometry. Bone. 2006;38:475–484.

74. Mulder L, Koolstra JH, Van Eijden TM. Accuracy of microCT in the quantitative determination of the degree and distribution of mineralization in developing bone. Acta Radiol. 2004;45:769–777.

75. Meganck JA, Kozloff KM, Thornton MM, Broski SM, Goldstein SA. Beam hardening artifacts in micro-computed tomography scanning can be reduced by X-ray beam filtration and the resulting images can be used to accurately measure BMD. Bone. 2009;45:1104–1116.

76. Kazakia GJ, Burghardt AJ, Cheung S, Majumdar S. Assessment of bone tissue mineralization by conventional x-ray microcomputed tomography: comparison with synchrotron radiation microcomputed tomography and ash measurements. Med Phys. 2008; 35:3170–3179.

77. Kohler T, Beyeler M, Webster D, Muller R. Compartmental bone morphometry in the mouse femur: reproducibility and resolution dependence of microtomographic measurements. Calcif Tissue Int. 2005;77:281–290.

78. Tommasini SM, Morgan TG, van der Meulen M, Jepsen KJ. Genetic variation in structure-function relationships for the inbred mouse lumbar vertebral body. J Bone Miner Res. 2005;20:817–827.

79. Tommasini SM, Wearne SL, Hof PR, Jepsen KJ. Percolation theory relates corticocancellous architecture to mechanical function in vertebrae of inbred mouse strains. Bone. 2008;42:743–750.

80. Hamrick MW, Pennington C, Newton D, Xie D, Isales C. Leptin deficiency produces contrasting phenotypes in bones of the limb and spine. Bone. 2004;34:376–383.

81. Judex S, Garman R, Squire M, Donahue LR, Rubin C. Genetically based influences on the site-specific regulation of trabecular and cortical bone morphology. J Bone Miner Res. 2004;19:600–606.

82. Leng H, Wang X, Ross RD, Niebur GL, Roeder RK. Micro-computed tomography of fatigue microdamage in cortical bone using a barium sulfate contrast agent. J Mech Behav Biomed Mater. 2008;1:68–75.

83. Chen RR, Snow JK, Palmer JP, et al. Host immune competence and local ischemia affects the functionality of engineered vasculature. Microcirculation. 2007;14:77–88.

84. Duvall CL, Taylor WR, Weiss D, Guldberg RE. Quantitative microcomputed tomography analysis of collateral vessel development after ischemic injury. Am J Physiol Heart Circ Physiol. 2004; 287:H302–310.

85. Duvall CL, Weiss D, Robinson ST, Alameddine FM, Guldberg RE, Taylor WR. The role of osteopontin in recovery from hind limb ischemia. Arterioscler Thromb Vasc Biol. 2008;28:290–295.

86. Waarsing JH, Day JS, van der Linden JC, et al. Detecting and tracking local changes in the tibiae of individual rats: a novel method to analyse longitudinal in vivo micro-CT data. Bone. 2004;34:163–169.

87. Boyd SK, Moser S, Kuhn M, et al. Evaluation of three-dimensional image registration methodologies for in vivo micro-computed tomography. Ann Biomed Eng. 2006;34:1587–1599.

88. Nishiyama KK, Campbell GM, Klinck RJ, Boyd SK. Reproducibility of bone micro-architecture measurements in rodents by in vivo microcomputed tomography is maximized with three-dimensional image registration. Bone. 46:155–161.

89. Campbell GM, Buie HR, Boyd SK. Signs of irreversible architectural changes occur early in the development of experimental osteoporosis as assessed by in vivo micro-CT. Osteoporos Int. 2008.

90. Buie HR, Moore CP, Boyd SK. Postpubertal architectural developmental patterns differ between the L3 vertebra and proximal tibia in three inbred strains of mice. J Bone Miner Res. 2008;23:2048–2059.

91. David V, Lafage-Proust MH, Laroche N, Christian A, Ruegsegger P, Vico L. Two-week longitudinal survey of bone architecture alteration in the hindlimb-unloaded rat model of bone loss: sex differences. Am J Physiol Endocrinol Metab. 2006;290:E440–447.

92. David V, Laroche N, Boudignon B, et al. Noninvasive in vivo monitoring of bone architecture alterations in hindlimb-unloaded female rats using novel three-dimensional microcomputed tomography. J Bone Miner Res. 2003;18:1622–1631.

93. Brouwers JE, Lambers FM, van Rietbergen B, Ito K, Huiskes R. Comparison of bone loss induced by ovariectomy and neurectomy in rats analyzed by in vivo micro-CT. J Orthop Res. 2009;27:1521–1527.

94. Brouwers JE, van Rietbergen B, Ito K, Huiskes R. Effects of vibration treatment on tibial bone of ovariectomized rats analyzed by in vivo micro-CT. J Orthop Res. 28:62–69.

95. Brouwers JE, van Rietbergen B, Bouxsein ML. Influence of early and late zoledronic acid administration on vertebral structure and strength in ovariectomized rats. Calcif Tissue Int. 2008;83:186–191.

96. Brouwers JE, van Rietbergen B, Huiskes R, Ito K. Effects of PTH treatment on tibial bone of ovariectomized rats assessed by in vivo micro-CT. Osteoporos Int. 2009;20:1823–1835.

97. Judex S, Luu YK, Ozcivici E, Adler B, Lublinsky S, Rubin CT. Quantification of adiposity in small rodents using micro-CT. Methods. 2010;50:14–19.

98. Dare A, Hachisu R, Yamaguchi A, Yokose S, Yoshiki S, Okano T. Effects of ionizing radiation on proliferation and differentiation of osteoblast-like cells. J Dent Res. 1997;76:658–664.

99. Klinck RJ, Campbell GM, Boyd SK. Radiation effects on bone architecture in mice and rats resulting from in vivo micro-computed tomography scanning. Med Eng Phys. 2008.

100. Guldberg RE, Lin AS, Coleman R, Robertson G, Duvall C. Microcomputed tomography imaging of skeletal development and growth. Birth Defects Res C Embryo Today. 2004;72:250–259.

101. Wang Y, Wan C, Deng L, et al. The hypoxia-inducible factor alpha pathway couples angiogenesis to osteogenesis during skeletal development. J Clin Invest. 2007;117:1616–1626.

102. Abruzzo T, Tumialan L, Chaalala C, et al. Microscopic computed tomography imaging of the cerebral circulation in mice: feasibility and pitfalls. Synapse. 2008;62:557–565.

103. Suo J, Ferrara DE, Sorescu D, Guldberg RE, Taylor WR, Giddens DP. Hemodynamic shear stresses in mouse aortas: implications for atherogenesis. Arterioscler Thromb Vasc Biol. 2007;27:346–351.

104. Awad HA, Zhang X, Reynolds DG, Guldberg RE, O'Keefe RJ, Schwarz EM. Recent advances in gene delivery for structural bone allografts. Tissue Eng. 2007;13:1973–1985.

105. Rai B, Oest ME, Dupont KM, Ho KH, Teoh SH, Guldberg RE. Combination of platelet-rich plasma with polycaprolactone-tricalcium phosphate scaffolds for segmental bone defect repair. J Biomed Mater Res A. 2007;81:888–899.

106. Mukundan S Jr, Ghaghada KB, Badea CT, et al. A liposomal nanoscale contrast agent for preclinical CT in mice. AJR Am J Roentgenol. 2006;186:300–307.

107. Nuzzo S, Lafage-Proust MH, Martin-Badosa E, et al. Synchrotron radiation microtomography allows the analysis of three-dimensional microarchitecture and degree of mineralization of human iliac crest biopsy specimens: effects of etidronate treatment. J Bone Miner Res. 2002;17:1372–1382.

108. Kinney JH, Ryaby JT, Haupt DL, Lane NE. Three-dimensional in vivo morphometry of trabecular bone in the OVX rat model of osteoporosis. Technol Health Care. 1998;6:339–350.

109. Burghardt AJ, Wang Y, Elalieh H, et al. Evaluation of fetal bone structure and mineralization in IGF-I deficient mice using synchrotron radiation microtomography and Fourier transform infrared spectroscopy. Bone. 2007;40:160–168.

110. Matsumoto T, Yoshino M, Asano T, Uesugi K, Todoh M, Tanaka M. Monochromatic synchrotron radiation muCT reveals disuse-mediated canal network rarefaction in cortical bone of growing rat tibiae. J Appl Physiol. 2006;100:274–280.

111. Raum K, Hofmann T, Leguerney I, et al. Variations of microstructure, mineral density and tissue elasticity in B6/C3H mice. Bone. 2007;41:1017–1024.

112. Schneider P, Stauber M, Voide R, Stampanoni M, Donahue LR, Muller R. Ultrastructural properties in cortical bone vary greatly in two inbred strains of mice as assessed by synchrotron light based micro- and nano-CT. J Bone Miner Res. 2007;22:1557–1570.